Swift ion irradiation effects on L-threonine amino acid single crystals



2007 J. Phys.: Condens. Matter 19 466108

(http://iopscience.iop.org/0953-8984/19/46/466108)

IOP PUBLISHING JOURNAL OF PHYSICS: CONDENSED MATTER

J. Phys.: Condens. Matter **19** (2007) 466108 (10pp) doi:10.1088/0953-8984/19/46/466108

# Swift ion irradiation effects on L-threonine amino acid single crystals

**G Ramesh Kumar[1], S Gokul Raj[1], V Mathivanan[1], M Kovendhan[1], R Mohan[1,3], Thenneti Raghavalu[1], D Kanjilal[2], K Asokan[2], A Tripathi[2], I Sulania[2] and Pawan K Kulriya[2]**

[1] Department of Physics, Presidency College, Chepauk, Chennai 600 005, India
[2] Inter-University Accelerator Centre, Aruna Asaf Ali Marg, New Delhi 110 067, India

E-mail: professormohan@yahoo.co.in

Received 5 June 2007, in final form 24 September 2007
Published 26 October 2007
Online at stacks.iop.org/JPhysCM/19/466108

**Abstract**

Single crystals of L-threonine were subjected to 50 MeV $Li^{3+}$ ion irradiation at various ion fluences. Radiation induced changes in the structural, electrical, thermal and optical properties of the crystals have been studied in detail. The ion fluence dependence on these properties has also been discussed. Surface modifications in the crystals have been explored through atomic force microscopy. It has also been observed that the powder second-harmonic generation efficiency of irradiated L-threonine varies with the ion fluence studied.

(Some figures in this article are in colour only in the electronic version)

## 1. Introduction

Amino acids are building blocks of proteins. In particular L-threonine is a neutral amino acid with chemical composition $CH_3$–CH(OH)–$CH(NH_2)$ COOH having a low density of 1.45 g $cm^{-3}$. L-threonine crystallizes in an orthorhombic system with four zwitterionic molecules per unit cell [1] linked by a three-dimensional network of N–H . . . O and O–H . . . O bonds. The non-centrosymmetric nature of many amino acid crystals plays a vital role in the field of non-linear optics [2, 3] as they have special features, like wide transparency in the UV as well as in the visible region, good thermal and mechanical strength, high second-harmonic generation (SHG) conversion efficiency etc; some amino acids like L-alanine, L-threonine produce radiolytic free radicals upon irradiation. In fact, crystalline L-alanine has proven to be a good candidate for applications in irradiation dosimetry [4, 5]. Keeping in view their various applications, the present work is aimed at the study of interactions of high energy ions with L-threonine molecular crystal. In our earlier reports [6–8], structural, optical, thermal and

[3] Author to whom any correspondence should be addressed.

  

second-order non-linear optical properties of L-threonine single crystals were studied in detail. Hence we concentrate on swift ion irradiation effects of L-threonine single crystals and the influence on the physical properties of irradiated crystals. The keV ion beam irradiation effects of L-alanine [9] and L-threonine [10], using $N^+$ and $He^+$ ions, have already been studied. In both cases, ion decomposition produces molecular emissions of $CO_2$, $H_2$ and $NH_3$.

## 2. Experimental procedure

### *2.1. Crystal growth and ion irradiation*

L-threonine single crystals were grown by both slow cooling and thermal evaporation techniques. Good quality crystals with well-defined morphology were cut into pieces of dimensions $5 \times 5 \times 1$ mm$^3$ and polished using alumina paste. 50 MeV $Li^{3+}$ ions from the 15 UD Pelletron [11] at the Inter-University Accelerator Centre (IUAC), New Delhi, India, were allowed to be incident on the crystalline sample mounted inside a 1.5 m diameter scattering chamber. The incident beam current was about 2 particle nanoamperes. The vacuum in the radiation chamber during the experiment was about $8 \times 10^{-7}$ mbar. The crystals were irradiated at various ion fluences, namely $1 \times 10^{10}$, $1 \times 10^{11}$ and $1 \times 10^{12}$ $Li^{3+}$ ions cm$^{-2}$, so as to study the fluence dependence on various physicochemical properties of the samples.

Usually, swift heavy ions (SHI) produced intense radiation damage in all materials which they traverse. The interaction between SHI and bulk materials leads to specific effects due to huge amounts of electronic energy $(dE/dx)_E$ being deposited on the target electrons by incident ions. In contrast, projectile/target nuclei collisions resulting in so called nuclear energy transfer $(dE/dx)_N$ play a lesser role for energetic heavy ions. These effects have been studied for a long time for insulators [12–14]. Both thermal spike [15] and pressure pulse/shock wave [16] models have been used for most materials to determine the sensitivity of materials to ion irradiations. The thermal spike model can also predict the threshold energy value of electronic energy loss of the ions for producing latent tracks in the materials. The latent tracks are supposed to be formed after rapid quenching of a cylindrical zone that has been melted along the ion path [17]. The electronic and nuclear energy losses suffered by the $Li^{3+}$ ion in L-threonine crystals were calculated using the transport of ions in matter (TRIM) program [18]. The projected range of 50 MeV $Li^+$ ions in L-threonine crystal was determined as 411 $\mu$m. Electronic and nuclear stopping powers of 50 MeV $Li^+$ ions for L-threonine were given using $(dE/dx)_E = 6.98$ eV Å$^{-1}$ and $(dE/dx)_N = 3.63 \times 10^{-3}$ eV Å$^{-1}$. Variations in electronic and nuclear energy losses of $Li^+$ ions for various incident energies are shown in figure 1.

### *2.2. Characterization studies*

Ion irradiation produces modification in bulk, localized and surface properties of the materials depending upon the irradiation dose, energy and atomic number of the ion beam and also on the properties of the target materials. The irradiated biomolecules of L-threonine, using $Li^{3+}$ ions at various ion fluencies, were treated using various tools like x-ray diffraction (Bragg–Brentano mode), UV–visible–NIR spectroscopy, dielectric studies, atomic force microscopy and Kurtz–Perry powder SHG measurements. Surface changes on irradiating the samples at various fluences were studied using a Bruker AXS D8 Advance x-ray diffractometer with Cu K$\alpha$, radiation. Transmittance spectra of both unirradiated and irradiated crystals were recorded using a Hitachi V-3300 UV–visible–NIR spectrophotometer in the wavelength range 190–1100 nm. Dielectric and AFM measurements on the irradiated samples were performed using a Solatron impedance analyser and a multimode SPM Nanoscope III A controller from

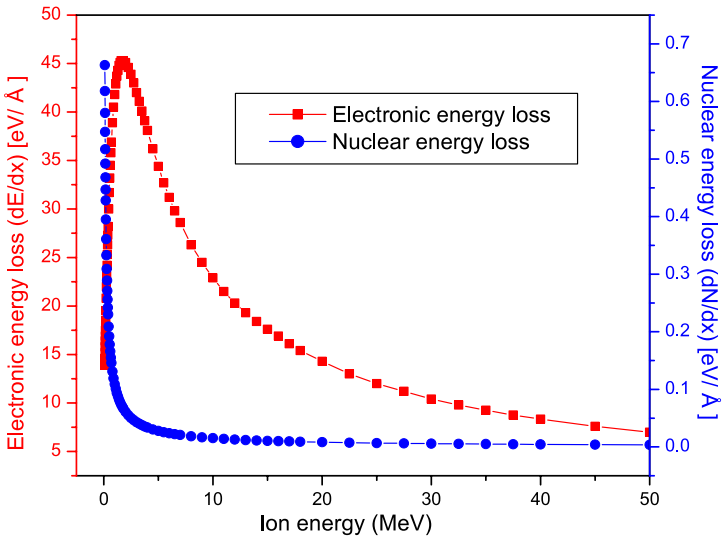


**Figure 1.** Nuclear and electronic energy losses for various input incident $Li^{3+}$ ion energies in L-threonine single crystals.

Digital/Vecco Instruments Inc. Powder SHG efficiencies for the irradiated samples of L-threonine were also measured for all ion fluences studied.

## 3. Results and discussion

### *3.1. X-ray diffractometry*

X-ray diffraction patterns of pristine (unirradiated) and irradiated samples of L-threonine were recorded in Bragg–Brentano (BB) geometry where the x-ray source and the detector move at equal angles. The scan speed was set as 0.02° $min^{-1}$ and the crystalline sample was also rotated at 4 rpm simultaneously. Figure 2 shows the x-ray diffractogram of L-threonine crystals irradiated at various $Li^{3+}$ ion fluences. As ion fluence increases, the degree of crystallinity of the irradiated samples decreases. For an ion fluence of $1 \times 10^{12}$ ions $cm^{-2}$, the surface of the crystal has lost its crystallinity completely and it shows that radiation induced amorphization occurred on the surface of the sample. The use of the BB mode in x-ray diffraction is more advantageous for single crystals as it varies the x-ray incidence angle and in the present case the angle of incidence varied up to 40°. From the density and absorption coefficient ($\alpha$) of L-threonine, the x-ray penetration depths were calculated at different incidence angles using an x-ray depth evaluation program [19] and the results are shown in figure 3. For an incidence angle of 40°, the x-ray penetration depth was found to possess a maximum value of 843 $\mu$m. Though it roughly estimates the amorphization depth of L-threonine irradiated at the higher fluence, TRIM calculation showed that the maximum projected range of the $Li^{3+}$ ion for the given energy was only around 411 $\mu$m. From these observations, it has been perceived that the amorphization depth exceeds the range ($R$) of the ions and it was approximately twice the $R$ value. In this range, electronic stopping is the most significant process and a large amount of energy would have been transferred into a relatively small volume causing an electronic avalanche and subsequently extending the damage region in the crystals. Deposition of a considerable amount of sputtered material on the surface of the sample [20] also accounts for the increased thickness of the amorphized layer.

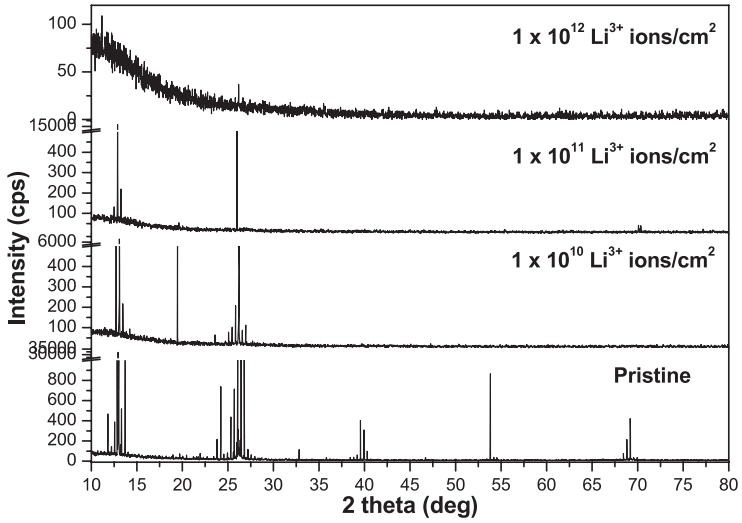


**Figure 2.** X-ray diffraction patterns of unirradiated and irradiated L-threonine single crystals at various ion fluences.

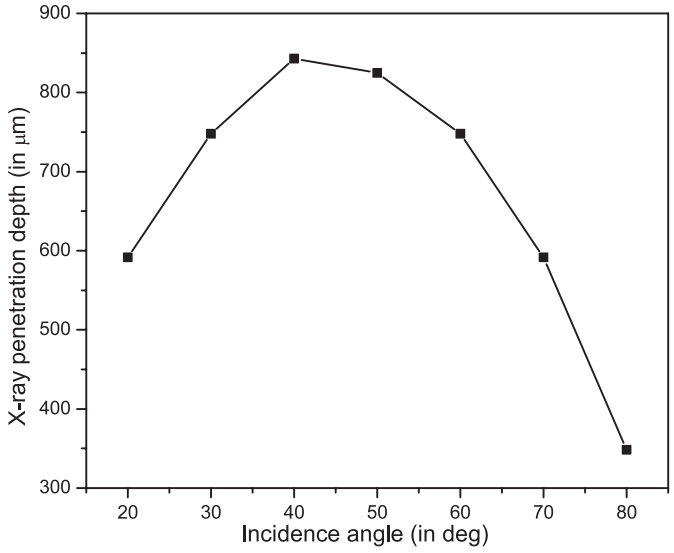


**Figure 3.** X-ray penetration depth of L-threonine single crystals at various incidence angles.

### *3.2. Atomic force microscopy*

Figures 4–6 show tapping mode normal incidence AFM images of $Li^{3+}$ ion irradiated L-threonine crystal at the fluences $1 \times 10^{10}$, $1 \times 10^{11}$ and $1 \times 10^{12}$ ions $cm^{-2}$. Samples bombarded at lower ion fluences of $1 \times 10^{10}$ ions $cm^{-2}$ show raised rims of height 0.85 nm and width 129.29 nm. For an ion fluence of $1 \times 10^{11}$ ions $cm^{-2}$, craters were also formed with a depth of 0.5 nm and a width of 169 nm. The metrology of craters and tails in the size range studied

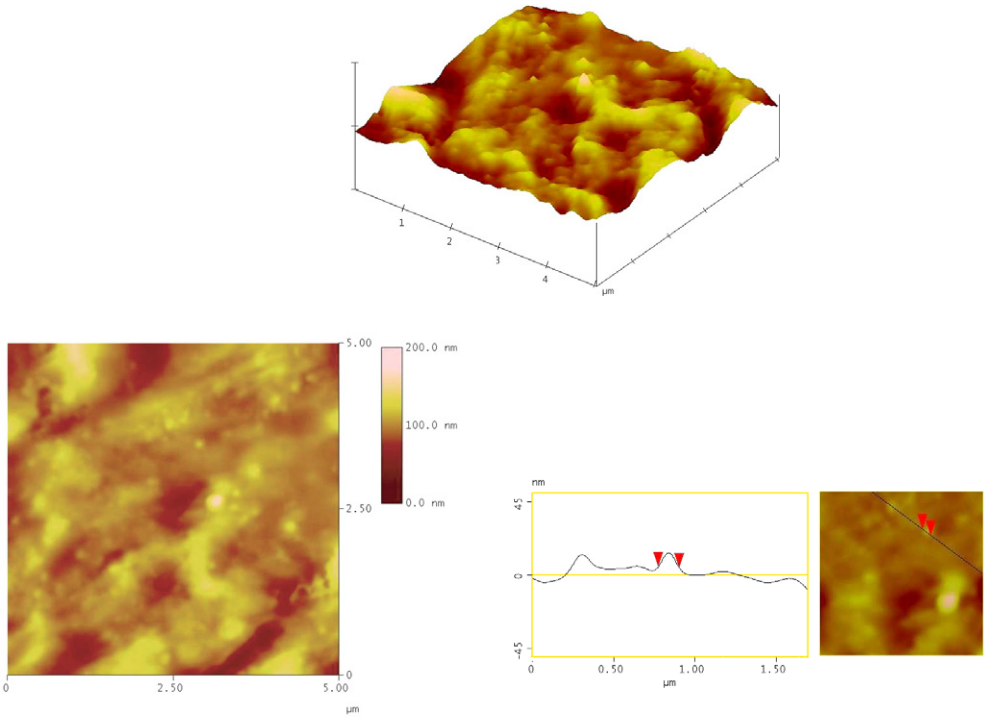


**Figure 4.** 3D and 2D AFM images of irradiated L-threonine at $1 \times 10^{10}$ ions cm$^{-2}$.

here on such soft biomolecules clearly presents a challenge for AFM technology. For normal incidence, the electronic energy deposited by an incident ion relaxes, depositing kinetic energy into the nuclear system. This may occur via Coulomb explosion along the ionized track; alternatively, secondary electrons emitted from the track may excite surrounding molecules and cause localized expansion of the specimen [21, 22]. Evaporation from the surface on a molecule-by-molecule basis could yield a crater. At both the extremities of the crater, the surface material does not receive enough momentum and highly energized underlying material attempts to eject and, as a result, a partial plastic deformation in the form of a bulge is induced on either side of a crater. At a higher fluence of $1 \times 10^{12}$ ions cm$^{-2}$, at the points for which the ion track is close to the surface, material would be receiving more than the critical impulse and can easily escape, leading to sputtering. However at the locations where the ion track is deeper, material receiving the critical impulse is impeded by the stationary material above, resulting in the observation of tail-like permanent plastic deformation along the ion track which indicates that a hydrodynamic pressure pulse occurs in response to the electronically deposited energy. As per the pressure pulse model [16], if the impulse to a volume of material exceeds a critical value, then a volume of material will get sputtered and, as a consequence, a hemispherical sputtered volume was predicated earlier [21]. A similar observation has also been reported for L-valine crystals [22, 23]. Following the various results, it has been concluded that the increased number of raised tails and bulges at the higher fluence of $1 \times 10^{12}$ ions cm$^{-2}$ multiplies the sputtering yield of neutral molecules and as well as producing radiation induced amorphization on the surface of the sample. The mean roughness values of the irradiated samples were also measured as 11.27, 45.72 and 18.66 nm for the ion fluences $10^{10}$, $10^{11}$

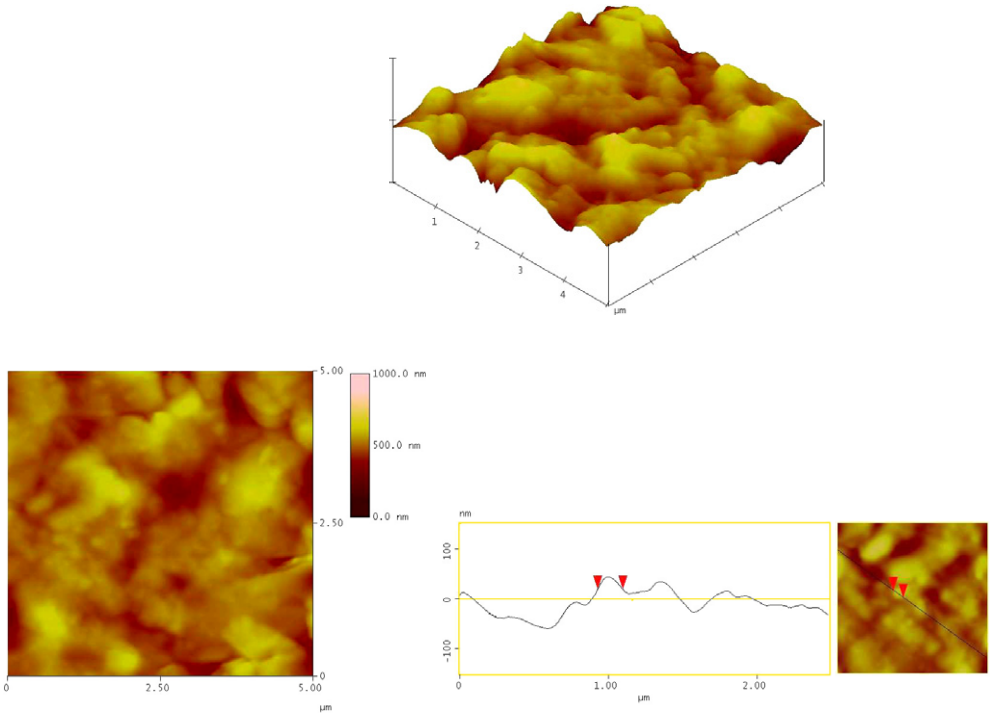


**Figure 5.** 3D and 2D AFM images of irradiated L-threonine at $1 \times 10^{11}$ ions $cm^{-2}$.

and $10^{12}$ whereas the pristine sample has a roughness of 7.3 nm. The decrease in the mean roughness at the higher fluence is mainly due to sputtering of a substantial amount of material per incident of MeV ion. Thus atomic force microscopy has provided a new and unique view of the intersection of the ion track with a surface and has elucidated the response of a material to a dense microscopic track of deposited energy.

### *3.3. Dielectric studies*

Dielectric permittivity and dielectric loss measurements were carried out for irradiated crystals of L-threonine in the frequency range 1 kHz–1 MHz at room temperature. Figures 7 and 8 show the dispersion of the dielectric constant and dissipation factor with ion fluence. At a lower fluence of $1 \times 10^{10}$ ions $cm^{-2}$, the dielectric constant decreases to 62 at 1 MHz. The decrease in dielectric constant may be due to the formation of small fragments including single atoms. Some of these, H, OH, CH and $CO_2$ etc, are volatile and readily de-gas from the sample. Simultaneous formation of a very large number of free radicals allows the movement of unpaired electrons within the molecules and increases the electrical conductivity of the sample. At a higher fluence of $1 \times 10^{12}$ ions $cm^{-2}$, the dielectric constant shot up suddenly due to amorphization of the sample surface. Finally it attained a steady state value of 191 for the entire frequency range studied. The dielectric loss values were found to be decreasing with increase in the ion fluences studied. It is well known that the electro-optic coefficient ($r_{ij}$) of any NLO molecular crystal depends on its dielectric constant and hence the irradiated crystals of L-threonine at a desired fluence can easily modulate its electro-optic properties. Thus ion irradiation of second-order NLO materials may easily be used to tune their $r_{ij}$ values.

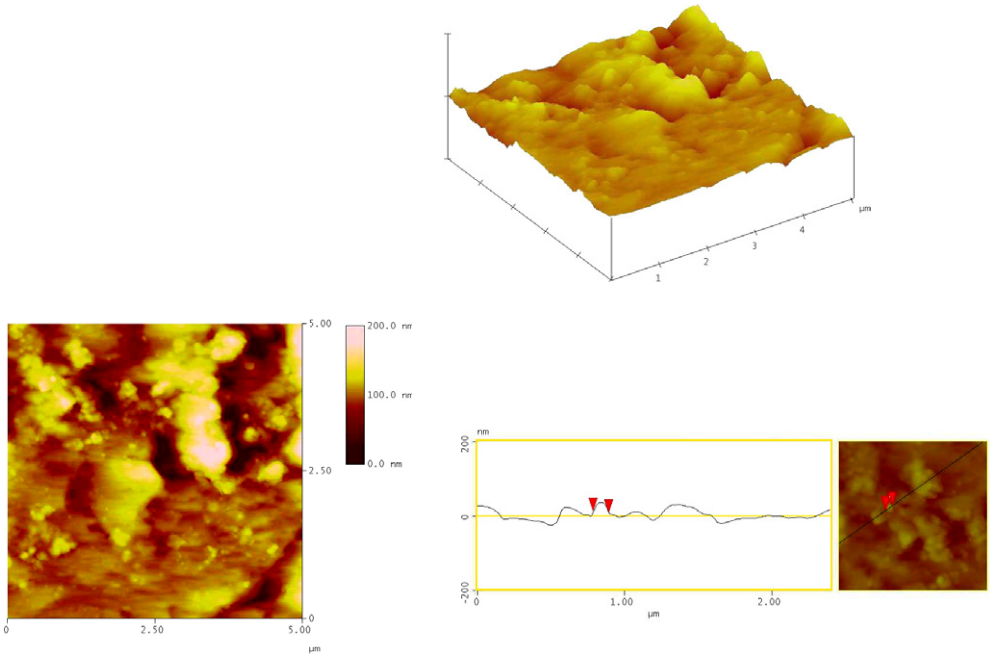

**Figure 6.** 3D and 2D AFM images of irradiated L-threonine at $1 \times 10^{12}$ ions $cm^{-2}$.

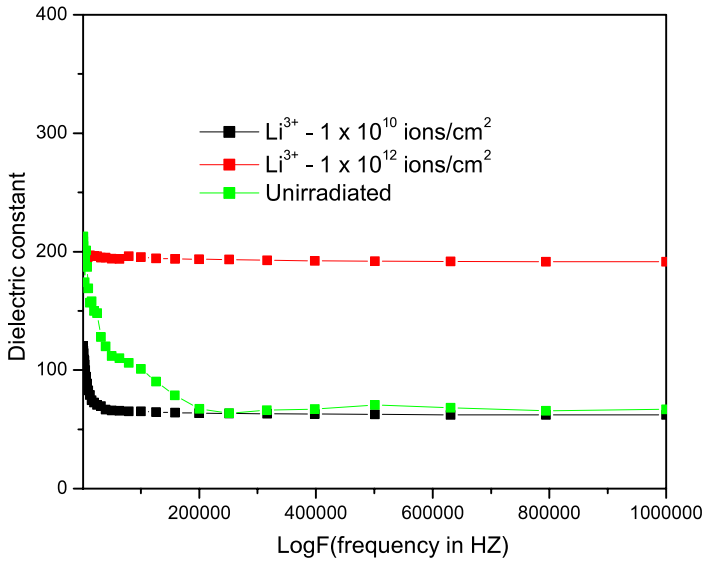


**Figure 7.** Dielectric constant of unirradiated and irradiated L-threonine single crystals at various ion fluences.

### *3.4. UV–visible–NIR spectroscopy*

UV–visible–NIR spectra recorded for unirradiated and irradiated crystals of L-threonine in the wavelength range 190–1100 nm show that there is a slight shift in the absorption edge towards the lower wavelength side for the higher fluence and this reflects the results obtained from the

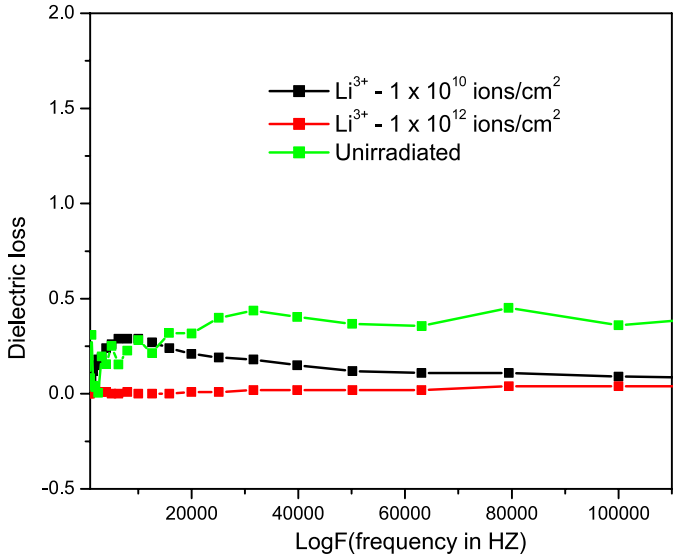


**Figure 8.** Dielectric loss of unirradiated and irradiated L-threonine single crystals at various ion fluences.

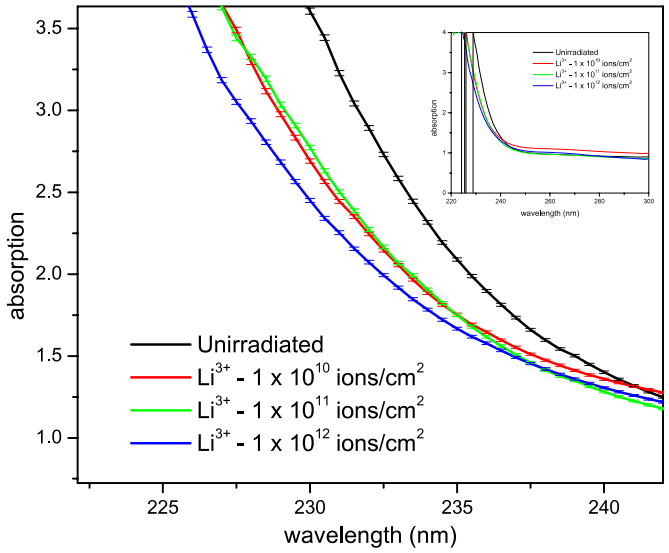


**Figure 9.** UV–visible–NIR spectra of unirradiated and irradiated L-threonine single crystals at various ion fluences.

dielectric measurements. The percentage of absorption also changed with the ion fluence and it is shown in figure 9.

### *3.5. Thermal analysis*

Simultaneous thermogravimetric and differential thermal analyses (TGA–DTA) were carried out for irradiated crystals of L-threonine ($1 \times 10^{11}$ ions $cm^{-2}$) in the temperature range

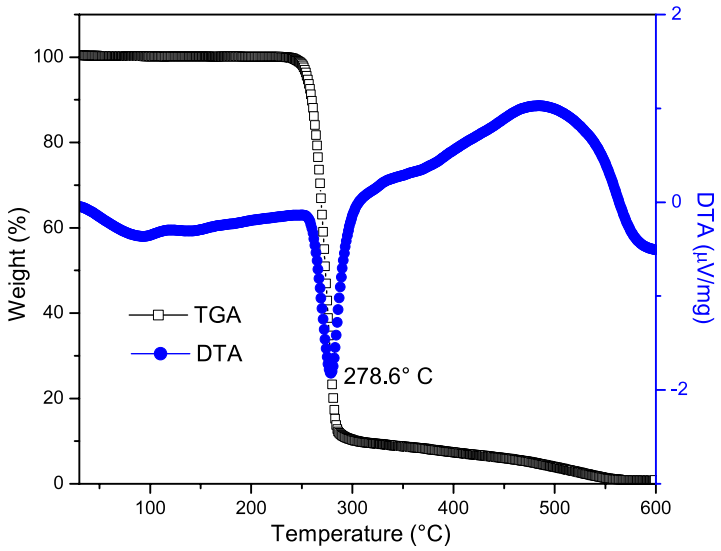


**Figure 10.** Simultaneous TGA–DTA for irradiated L-threonine single crystals at $1 \times 10^{11}$ ions $cm^{-2}$.

30–600 °C at a heating rate of 5 °C $min^{-1}$ in nitrogen atmosphere; see figure 10. A sudden weight loss and an endothermic thermal event at 278.6 °C in TGA and DTA show the decomposition temperature of irradiated L-threonine, while for an unirradiated crystal, the decomposition was reported as 265.2 °C [8]. The increase in thermal stability is due to decrease in the degree of crystallinity of the irradiated samples.

### *3.6. Kurtz–Perry powder SHG measurement*

The second-harmonic generation conversion efficiency for both unirradiated and irradiated polycrystalline samples of L-threonine were measured relative to potassium dihydrogen phosphate (KDP). The instrument used was an Nd:YAG laser of wavelength 1064 nm with pulse width of 10 ns and a repetition rate of 10 Hz. The average grain sizes were found to be same for all the unirradiated and irradiated samples with different ion fluences. At lower ion fluences, the powder SHG efficiency of L-threonine did not show appreciable variation, but for higher fluence, say for $10^{11}$ and $10^{12}$ ions $cm^{-2}$, the SHG output drastically reduced to half of its original value. This may be due to the fact that the higher dose of irradiation has considerably affected the non-centrosymmetric packing of the molecular crystal.

## 4. Conclusions

L-threonine single crystals were irradiated with 50 MeV $Li^{3+}$ ions at various ion fluences. X-ray diffraction study confirms the amorphization phenomena occurring on the surfaces of crystals at the higher fluence. Atomic force microscopy of irradiated crystals shows that interaction of high energy ions with soft biomolecules leads to the ejection of intact molecules through a sputtering mechanism. The tail-like appearance of the AFM images at the higher fluences indicates the permanent plastic deformation of the surface of the crystals. Dielectric studies reveal that the dielectric constant decreases at the lower fluence and increases suddenly for the higher fluences due to amorphization. Ion irradiation of L-threonine also affects its

transmittance properties. The thermal strength of irradiated L-threonine was found to be higher than that of unirradiated L-threonine. Powder SHG measurements show that the second-harmonic output decreases for higher fluences and hence NLO properties of crystals were marginally affected by ion irradiation.

## Acknowledgments

The authors, G Ramesh Kumar and S Gokulraj, wish to thank the Council of Scientific and Industrial Research (CSIR), New Delhi, India, for awarding a Senior Research Fellowship (SRF) and an Extended Senior Research Fellowship (Ext-SRF).

## References

[1] Shoemaker D P, Donohye J, Shoemaker V and Corey R B 1950 *J. Am. Chem. Soc.* **72** 2328
[2] Rodrigues J J Jr, Misoguti L, Nunes F D, Mendonca C R and Zilio S C 2003 *Opt. Mater.* **22** 235
[3] Razetti C, Ardoino M, Zanotti L, Zha M and Paorici C 2002 *Cryst. Res. Technol.* **37** 456
[4] Winkler E, Etchegoin P, Fainstein A and Fainstein C 1998 *Phys. Rev.* B **57** 13477
[5] Ebraheem S, Beshir W B, Eid S, Sobhy R and Kovacs A 2003 *Radiat. Phys. Chem.* **67** 569
[6] Ramesh Kumar G, Gokul Raj S, Sankar R, Mohan R, Pandi S and Jayavel R 2004 *J. Cryst. Growth* **267** 213
[7] Ramesh Kumar G, Gokul Raj S, Mohan R and Jayavel R 2006 *Cryst. Growth Des.* **6** 1308
[8] Ramesh Kumar G, Gokul Raj S, Raghavalu T, Mathivanan V, Kovendhan M, Bhagavannarayana G and Mohan R 2007 *Mater. Lett.* **61** 4932
[9] Foti A M, Milano F and Torrisi L 1990 *Nucl. Instrum. Methods* B **46** 361
[10] Huang W, Yu Z and Zhang Y 1998 *Nucl. Instrum. Methods* B **134** 202
[11] Mehto G K and Patro A P 1988 *Nucl. Instrum. Methods Phys. Res.* A **268** 334
[12] Balanzet E 1993 *Radiat. Eff.* **126** 97
[13] Matzke H 1983 *Radiat. Eff.* **64** 3
[14] Toulemonde M, Bouffard S and Studer F 1994 *Nucl. Instrum. Methods* B **91** 108
[15] Wang Z G, Dufour Ch, Paumier E and Toulemonde M 1994 *J. Phys.: Condens. Matter* **6** 6733
[16] Johnson R E *et al* 1989 *Phys. Rev.* B **40** 49
[17] Fleischer R L, Price P B and Walker R M 1975 *Nuclear Tracks in Solids: Principles and Applications* (Berkeley, CA: University of California Press)
[18] Ziegler J F, Biersack J D and Littmark U 1988 *The Stopping and Ranges of Ions in Solids* (New York: Pergamon)
[19] Zanola P, Colombi P, Bontempi E, Gelfi M, Roberti R and Depero L E 2006 *J. Appl. Crystallogr.* **39** 176
[20] Rozlosnik N, Sajo Bohus L, Birattar C, Gadioli E, Biro L P and Havancsak K 1997 *Nanotechnology* **8** 32
[21] Fenyo D and Johnson R E 1992 *Phys. Rev.* B **46** 5090
[22] Kopniczky J, Reimann C T, Hallen A, Sundqvist B U R, Tengvall P and Erlandrson R 1994 *Phys. Rev.* B **49** 625
[23] Kopniczky J, Hallen A, Kesikitaloo N, Reimann C R and Sundqvist B U R 1995 *Radiat. Meas.* **25** 47